Communication

A Dual-Band Guided-Laser Absorber Based on Silicon-Nickel Metasurface

Xinye Liao [1], Junxiang Zeng [1], Yunxiang Zhang [1], Jianjing Zhao [1], Xin He [2],* and Junbo Yang [2]

1   Undergraduate School, National University of Defense Technology, Changsha 410073, China
2   Department of Physics, National University of Defense Technology, Changsha 410073, China
*   Correspondence: hexin12a@nudt.edu.cn

Abstract: Metasurface absorbers are already used in many laser applications. To achieve laser stealth, a dual-band guided-laser absorber is presented in this paper. The absorber is composed of periodic silicon squares on a silicon film and a nickel layer. Under normal incidence, the absorber has two absorption peaks at wavelengths of 1.55 µm and 1.064 µm, with absorption rates higher than 94.4%. For wavelength-tunable 1.55 µm lasers with a large wavelength tuning range of ±50 nm, the absorption rate is still as high as 90%. Plasmonic resonance theory, as well as FDTD simulations, are used to design and study the absorber. It is found that the absorber is independent of the incident polarization and tolerant to the incident angle. The design method is flexible, and the absorber is easy to manufacture.

Keywords: metasurface; laser stealth; dual-band absorption; grating

1. Introduction

In recent years, infrared laser guidance has employed multi-wavelength lasers working together [1]. Under the irradiation of multi-wavelength lasers, targets need to reduce their surface reflection, so as to achieve "laser stealth". At present, there are two main ways to reduce reflection. One is to improve absorption with the help of absorbing materials; the other is to utilize light guide and/or light transmission effects. So far, a variety of laser-stealth materials have been developed. These materials include coated laser-absorbing materials, nano-absorbing materials, semiconductor compounds, and spectral conversion materials [2]. It is difficult to achieve laser stealth based on light guide and/or light transmission effects. Therefore, great effort has been devoted to research related to absorbing materials.

Recently, metamaterials have opened up new directions for polarization detection, sensing [3,4] and infrared laser-absorbing materials. Various metamaterials, such as gradient metasurfaces [5], typed porous metasurfaces [6], and circular hole array metasurfaces [7], have been proposed. Typically, metamaterials consist of large numbers of artificial "atomic" microstructures. Since Pendry et al. [8,9] proposed electromagnetic stealth metamaterials and perfect lenses, stealth materials based on metamaterials have emerged one after another. For example, Cheng et al. [10] presented a non-resonant "I"-shaped metamaterial and a resonant ELC metamaterial, which demonstrate 99% absorption at microwave frequencies. Nie et al. [11] proposed a two-layer asymmetric split-ring metamaterial that exhibits efficient multi-band absorption. Kadir et al. [12] achieved ~90% absorption in the entire long-wave infrared (LWIR) by burying two parallel metasurfaces in an amorphous silicon layer. However, there are few studies on laser-absorbing metamaterials. Many metamaterial absorbers suffer from the disadvantages of a single absorption band [13], polarization sensitivity [14], and only being suitable for normal incidence [15].

In particular, 1.55 µm lasers have been applied to achieve precise guidance [16], which presents new challenges in the study of laser-absorbing metamaterials. This is because 1.55 µm lasers usually have wavelength tuning capabilities. In the face of wavelength

tuning, if the metamaterial covering the target surface cannot maintain high absorption within the tuning range of the incident laser, the target will barely survive [17]. To address this problem, some researchers have investigated the use of Helmholtz resonators [18]. However, Helmholtz resonators operating at light frequencies are difficult to manufacture.

In the study of solar energy harvesting, researchers have found that two-dimensional gratings can produce high absorption of visible light [19]. Inspired by this, we design and investigate a dual-band laser absorber based on Si-Ni metasurface. It can efficiently absorb the 1.55 μm and 1.064 μm lasers, providing a way of achieving laser stealth. For a recent 1.55 μm laser with a wavelength tuning range of 60 nm [20], the metasurface can maintain an absorptivity greater than 93%. In addition, the metasurface has a low emissivity in the mid-infrared range, showing good thermal stealth performance under night conditions [21]. To understand the underlying mechanism, electromagnetic field distributions, energy loss distributions, and effective impedance are investigated. Moreover, considering the fabrication error and practical applications, the effects of geometric parameters, polarization of incidence, and incident angle on the absorption performance are discussed.

2. Structure Design

Figure 1 shows the proposed metasurface based on Si-Ni microstructures. It is a two-dimensional periodic structure consisting of three functional layers. In each unit cell of the metasurface, there is a continuous silicon film between a silicon square and a nickel layer, as shown in Figure 1a. The period of the metasurface is p, and the side length of the square is d, as shown in Figure 1b. The thicknesses of the square, the continuous silicon film, and the nickel film are h_1, h_2, and h_3, respectively, as shown in Figure 1c. We chose silicon because of its high refractive index, which can improve tolerance to oblique incidence. Nickel is use due to its relatively high loss at the wavelengths of interest, which can enhance absorption. The nickel film must be thick enough to prevent the penetration of incident light. In our structure, it has a thickness of 100 nm (i.e., $h_3 = 100$ nm). Please note that there is a substrate (not shown) under the nickel film. The substrate (such as a polished silicon wafer) only acts as a support. It has no effect on the performance of the metasurface.
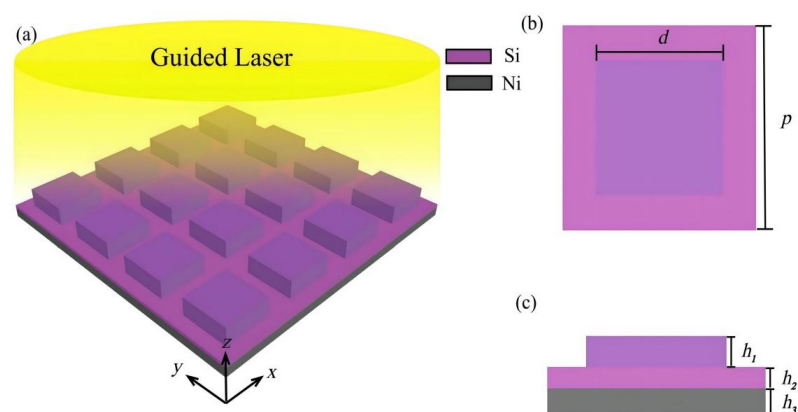

Figure 1. Schematic diagram of the metasurface. (**a**) 3D view of the metasurface. (**b**) Top view of each unit cell. (**c**) Side view of each unit cell.

When the metasurface is illuminated by a laser, surface plasmon polaritons (SPPs) could be excited. According to the wavevector matching theory [22,23], whether or not to excite the SPP is controlled by:

$$\left| \beta_{\parallel}^{(\pm m)} \right| = \left| k_{\parallel} \pm m k_g \right| \tag{1}$$

where $\beta_{\parallel}$ and $k_{\parallel}$ are respectively the in-plane wavevector of the SPP and the incident light, k_g is the grating vector, m is a positive integer. The thickness of the silicon square is small,

so only (+1) and (−1) SPP modes will be excited. Assuming that the polarization of the incident light is along the x-direction, Equation (1) can be expressed as:

$$\frac{2\pi n_{eff}^{(\pm 1)}}{\lambda^{(\pm 1)}} = \frac{2\pi}{\lambda^{(\pm 1)}} \sin\alpha \pm \frac{2\pi}{p} \tag{2}$$

where n_{eff} is the effective refractive index of the SPP mode, λ is the free-space wavelength, and α is the incident angle. It is similar if the polarization of the incident light is along the y-direction.

Since silicon has a high refractive index, localized plasmon resonance may also be excited [24,25]. According to the impedance matching theory [26], when the radiative and resistive losses of the eigenmode equal to each other, critical coupling can occur. In this situation, if the incident light excites the eigenmode due to the radiation coupling, the incident energy will be completely converted into the ohmic loss, leading to perfect absorption. The absorption rate $A(\lambda)$ can be expressed as:

$$A(\lambda) = 1 - \left| \frac{Z(\lambda) - 1}{Z(\lambda) + 1} \right|^2 \tag{3}$$

where $Z(\lambda)$ is the effective impedance of the metasurface.

To optimize the structural parameters and achieve near-perfect dual-band laser absorption, finite-difference time-domain (FDTD) simulations were carried out. The optical parameters of silicon and nickel were taken from the literature [27].

Figure 2 plots the absorbance, reflectivity and transmittance of the metasurface under normal incidence. The geometric parameters are as follows: $p = 856$ nm, $d = 550$ nm, $h_1 = 60$ nm, $h_2 = 36$ nm, $h_3 = 100$ nm. As can be seen in Figure 2, the transmittance is almost zero in the investigated spectral range. The reflectance has two dips centered at wavelengths of 1.064 µm and 1.55 µm, respectively. The absorptivity of the metasurface satisfies $A = 1 - R - T$, where R and T are the reflectance and transmittance, respectively. Therefore, the absorptivity is ~97.8% and ~94.4% at 1.064 µm and 1.55 µm wavelengths, respectively. The results indicate that the metasurface can achieve high absorption of dual-band guided laser. Especially for the 1.55 µm band, the metasurface can still maintain >90% absorbance even when the wavelength tuning range of the laser reaches ±50 nm. It implies that our absorber has the ability to counteract the wavelength tuning.
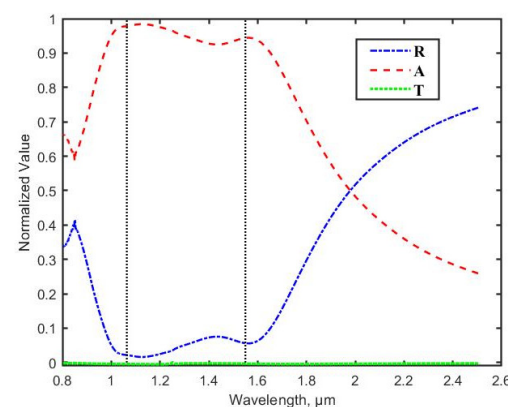

Figure 2. Calculated absorbance (A), reflectivity (R), and transmittance (T) of the metagrating. The two vertical dashed lines mark the 1.064 µm and 1.55 µm wavelengths, respectively.

3. Absorption Mechanism

To understand the absorption mechanism, the distributions of electric field $|E|$ and magnetic field $|H|$ at the resonance wavelengths were studied. The results are shown in Figure 3. In Figure 3a,c, we observe that the electric field is mainly confined in the gap between adjacent squares. The magnetic field mainly distributes in the continuous

silicon layer, and is relatively strong below the gap. This is because the free electrons in the nickel layer form an oscillating current. In other words, propagating plasmonic resonance is excited. However, there is a portion of the magnetic field below the square, implying some degree of localized plasmonic resonance. Therefore, the absorption at the 1.064 μm wavelength can be attributed to a mixed mode, which is dominated by propagating plasmonic resonance and supplemented by localized plasmonic resonance. In Figure 3b,d, it can be seen that the electric field is mainly associated with the square. Meanwhile, the magnetic field is strongly concentrated below the square. These phenomena are consistent with localized plasmonic resonance. However, a small portion of the magnetic field leaks out. Therefore, the absorption at the 1.55 μm wavelength is also a mixed mode, which is dominated by localized plasmonic resonance and supplemented by propagating plasmonic resonance.
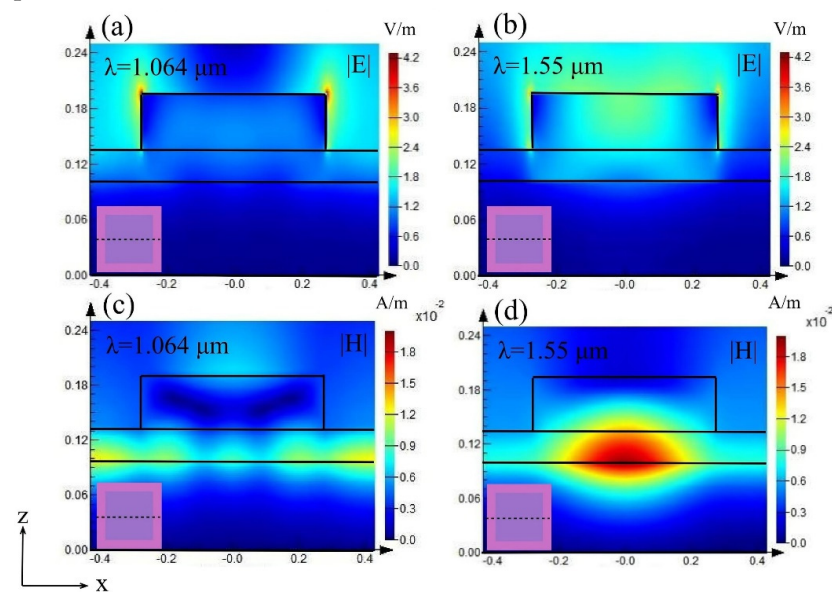

Figure 3. Cross-sectional view of the electromagnetic field distributions. (**a**,**c**) Electric and magnetic field distributions at the wavelength of 1.064 μm, respectively. (**b**,**d**) Electric and magnetic field distributions at the wavelength of 1.55 μm, respectively. Insets show the location of the cross-section.

Then, the permittivity, permeability, effective refractive index and effective impedance of the metasurface were retrieved [28], as shown in Figure 4. In Figure 4a,c, it can be seen that Im(ε) and Im(μ) are positive and large at wavelengths of 1.064 μm and 1.55 μm, indicating magnetic resonance. Meanwhile, Im(ε) is positive and large at the two wavelengths, indicating high loss. According to $Z(\lambda) = \sqrt{\mu(\lambda)/\varepsilon(\lambda)}$, we can obtain the effective impedance of the metasurface, as shown in Figure 4d. For the wavelength of 1.064 μm, Re(Z) is relatively large and close to 1, and Im(Z) is approximately 0. For the wavelength of 1.55 μm, Re(Z) is close to 1, and Im(Z) is a relative maximum. These indicate that the impedance of the metasurface is matched to the free space at wavelengths of 1.064 μm and 1.55 μm, resulting in reduced reflections. Therefore, at 1.064 μm and 1.55 μm wavelengths, the loss increases and the reflection decreases, leading to an increase in absorption. However, since Z does not reach 1, there will be little reflection, and the absorption does not reach 100%.

Because the structure in each unit cell is symmetric, absorption properties will not depend on the polarization of the incidence [29]. Assuming a TM-polarized (the polarization is along the x-direction) incidence, Figure 5 shows the energy dissipation in the nickel film. A cross-section close to the upper surface of the nickel film was studied, as shown in Figure 5a. In Figure 5b, for the wavelength of 1.064 μm, the energy loss occurs mainly below the gap between adjacent squares. A small portion of energy dissipates below the square. This is due to the oscillation of free electrons in the nickel film, which is consistent with the electromagnetic field distributions in Figure 3. Similarly, in Figure 5c,

for the wavelength of 1.55 μm, the energy loss occurs mainly below the square. This is also consistent with the electromagnetic field distributions in Figure 3.
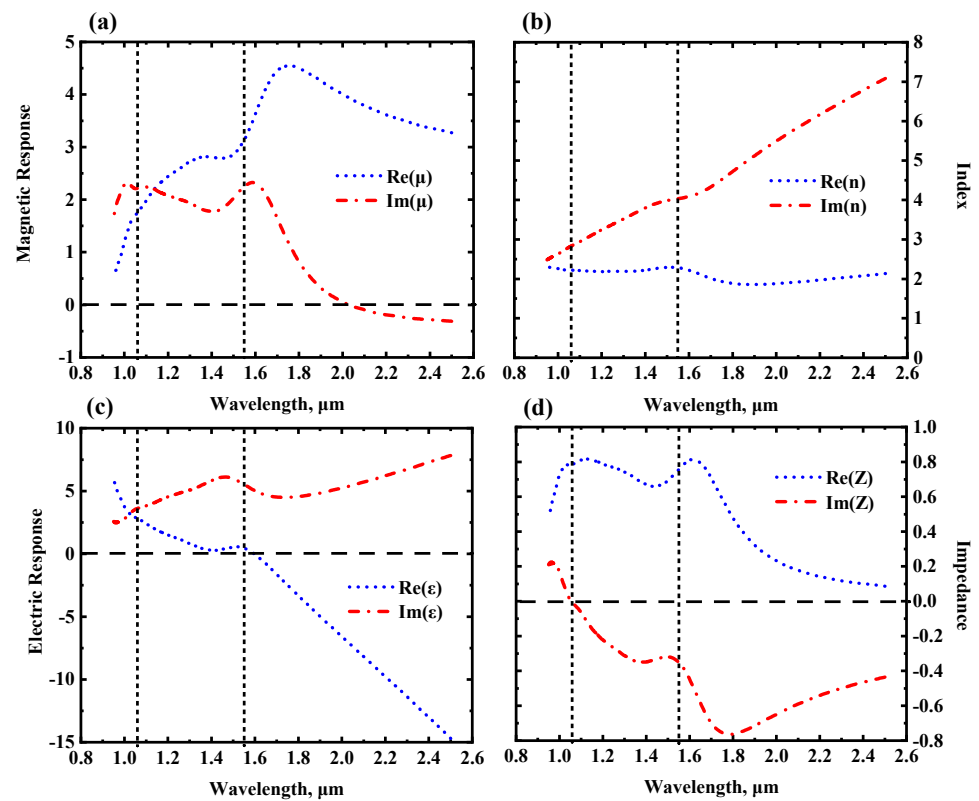

Figure 4. Effective optical constants of the metasurface. (**a**) Magnetic permeability. (**b**) Refractive index. (**c**) Permittivity. (**d**) Impedance. Please note that 'Re' represents the real part and 'Im' represents the imaginary part.
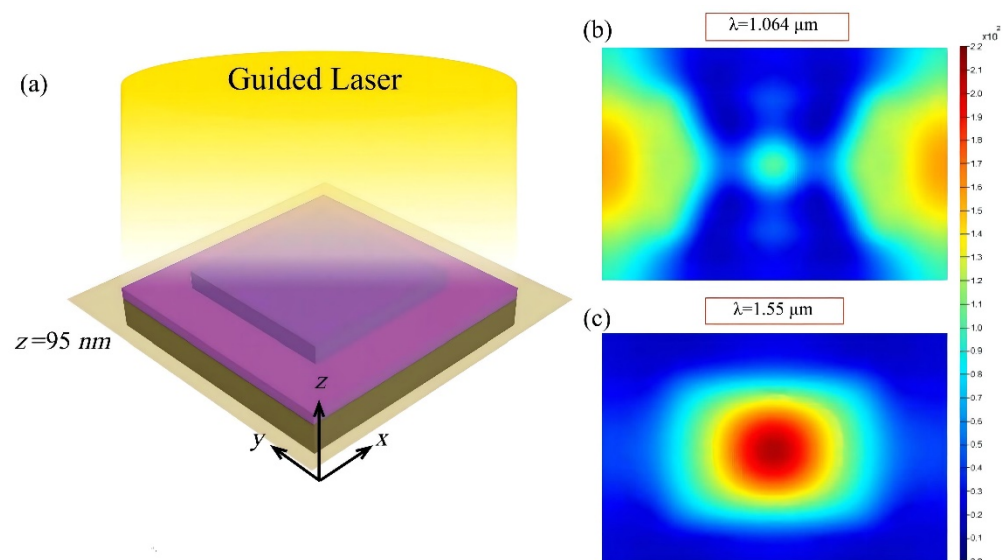

Figure 5. Simulated energy loss at the 1.064 μm and 1.55 μm wavelengths. (**a**) Position of the investigated cross-section. (**b,c**) Energy losses at wavelengths of 1.064 μm and 1.55 μm, respectively. The distance between the cross-section and the bottom surface of the nickel film is 95 nm.

4. Discussion

The absorber is easily fabricated by micro-nanotechnology. The following method can be used to prepare the absorber. First, by means of vacuum evaporation, a layer of nickel

and a silicon film can be sequentially coated on a substrate. Then, a layer of E-beam resist is spin-coated on top of the silicon film. Using E-beam lithography, the desired squares can be patterned. After developing and fixing, a sample with periodic square holes will be obtained. Next, an additional layer of silicon is evaporated on the sample. Removing the E-beam resist, we can obtain the proposed absorber.

To analyze the influence of manufacturing errors, the absorption spectra were simulated by adjusting the geometric parameters d, p, h_1, and h_2 (see Figure 1). Since the proposed metasurface is polarization independent, the absorption performance is discussed by taking a TM-polarized incidence as an example. The thickness of the nickel film (i.e., h_3) is not discussed.

Figure 6 shows the calculated absorption when a single geometric parameter is adjusted with other parameters unchanged. For ease of discussion, the peaks around the wavelength of 1.064 μm are marked as M_1, whereas the peaks around the wavelength of 1.55 μm are marked as M_2.
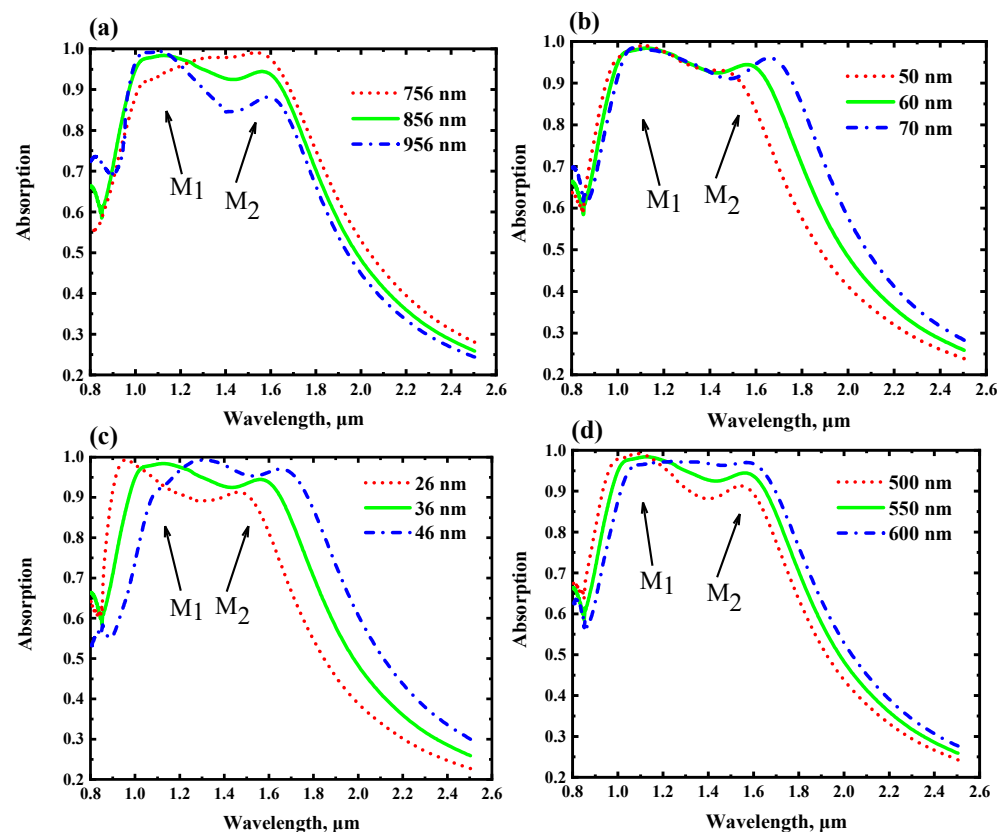

Figure 6. Effects of changing geometric parameters. (**a**) Changing the period. (**b**) Changing the thickness of the continuous silicon layer. (**c**) Changing the thickness of the silicon square. (**d**) Changing the side length of the silicon square.

Figure 6a shows the absorption spectra as a function of p. A change in p implies a change in the gap, which affects the near-field coupling between adjacent squares. When $p = 756$ nm, the absorption at M_1 decreases due to the increased in the duty cycle of the top grating. Owing to the small gap, the near-field coupling becomes strong, and the absorption peaks degenerate. In this situation, the impedance is not perfectly matched to the free space. When p decreases from 956 nm to 856 nm, M_1 does not change significantly, whereas the absorption at M_2 increases significantly. It is indicated that an appropriate period will enhance the resonance.

Figure 6b shows the absorption spectra as a function of h_1. It can be observed that changing h_1 has little effect on the absorption at M_1. When h_1 increases from 50 nm to

70 nm, M_2 exhibits a slight red shift, indicating that increasing h_1 can tune the position of M_2 to a certain extent.

Figure 6c shows the absorption spectra as a function of h_2. When $h_2 = 26$ nm, the two peaks are blue-shifted to 0.96 μm and 1.46 μm, respectively. This is because the coupling between the upper and lower layers is enhanced. Meanwhile, the impedance is not well matched to the free space. When $h_2 = 36$ nm, the absorption is high. The reason for this is that the coupling between the upper and lower layers is weakened (the impedance matching is better). However, when $h_2 = 46$ nm, the two peaks are red-shifted to 1.31 μm and 1.66 μm, respectively. In this situation, high absorption at the 1.064 μm wavelength cannot be obtained.

Figure 6d shows the absorption spectra as a function of d. As d increases, the absorption at M_2 increases, whereas the absorption at M_1 decreases. When $d = 600$ nm, the two peaks tend to degenerate. This is because the two resonances tend to influence each other as d increases.

In practical applications, the response to the angle of incidence needs to be considered. Figure 7 shows the spectral response of the metasurface at different angles of incidence. As the incident angle increases, the absorption rate decreases to a certain extent. For the peak at the wavelength of 1.064 μm, its absorption rate remains ≥85% at incident angles up to 60 degrees. For the peak at the wavelength of 1.55 μm, its spectral location exhibits a blue shift at oblique incidence. When the incident angle is as high as 60 degrees, the absorption at the 1.55 μm wavelength is still ≥75%. The results show that the metasurface is tolerant to the incident angle. In particular, at large incident angles, if the 1.55 μm laser performs wavelength tuning (±50 nm), the metasurface can still have an absorptivity of ≥70%.
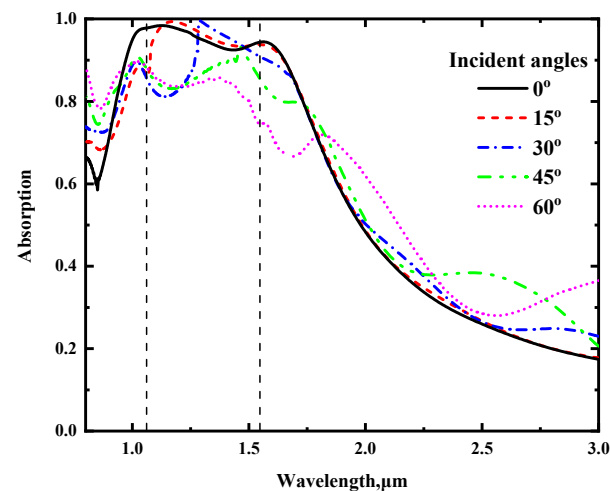

Figure 7. Absorption spectra at different angles of incidence.

Moreover, the response to the polarization of incidence is also an important property of the metasurface. Figure 8 illustrates the absorption spectra at different polarization angles. In Figure 8, "0°" represents that the polarization of the incidence is along the x-direction; and "90°" represents that the polarization of the incidence is along the y-direction. As can be observed, when the polarization varies, absorption spectra of the metasurface remain almost unchanged. These results suggest that the metasurface is polarization insensitive.

It is well known that passive infrared detection (detecting the thermal radiation of a target) is a common and important detection method under night conditions. Figure 9 plots the reflection of the metasurface in the mid-infrared. It is obvious that, in addition to high absorption of the 1.064 μm and 1.55 μm lasers, the reflectivity is ≥80% at wavelengths greater than 2.8 μm. As mentioned above, the thick nickel layer cannot transmit (infrared) light. Therefore, the observed high reflectivity is associated with low absorptivity for thermal infrared. According to Kirchhoff's law, the low absorptivity means a low thermal emissivity. For a given temperature, the thermal infrared radiation intensity of a target

coated with our metasurface is relatively small. Therefore, under night conditions, the proposed metasurface is useful for circumventing passive infrared detection.
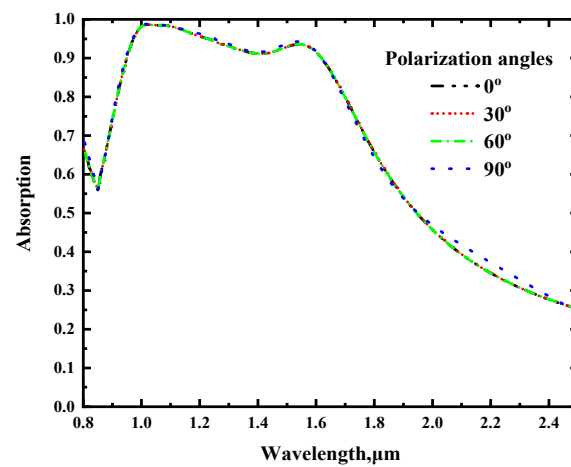

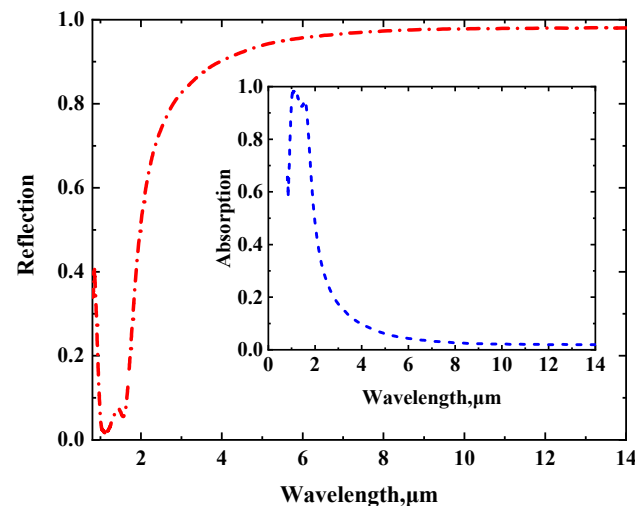**Figure 8.** Absorption spectra at different polarization angles.

Figure 9. Reflection and absorption at mid-infrared frequencies.

5. Conclusions

A dual-band guided laser-absorbing metasurface was designed and numerically studied. The metasurface consists of silicon squares on a continuous silicon layer and a nickel film. According to FDTD simulation results, at normal incidence, the absorption can reach 97.8% at the wavelength of 1.064 μm and 94.4% at the wavelength of 1.55 μm. In particular, for an incident 1.55 μm laser with a wavelength tuning range of ±50 nm, the metasurface can always maintain a high absorption rate of ≥90%. By analyzing the electromagnetic field distributions and energy dissipation, it was found that the resonances contain localized plasmonic resonance and propagating plasmonic resonance. Both resonances contribute to the absorption, but the dominant resonance at the wavelength of 1.064 μm is different from that at the wavelength of 1.55 μm. The geometric parameters in each unit cell have a significant effect on the absorption performance. The metasurface was shown to be polarization independent and tolerant to the incident angle. Fabrication of the metasurface is easy and compatible with current CMOS technology. Therefore, the metasurface is low cost, and is useful in laser stealth applications.

Institutional Review Board Statement: Not applicable.

Informed Consent Statement: Not applicable.

Data Availability Statement: The data presented in this study are available on request from the corresponding author.

References

1. Shen, X.P.; Yang, Y.; Zang, Y.Z.; Gu, J.Q.; Han, J.G.; Zhang, W.L.; Cui, T.J. Triple-band terahertz metamaterial absorber: Design, experiment, and physical interpretation. *Appl. Phys. Lett.* **2012**, *15*, 1–4. [CrossRef]
2. Zhao, J.; Chen, H.S.; Wang, J.L. Laser stealth materials and its developments tendency. *Dev. Appl. Mater.* **2011**, *5*, 78–82.
3. Butt, M.A.; Khonina, S.N.; Kazanskiy, N.L.; Piramidow, R. Hybrid metasurface perfect absorbers for temperature and biosensing applications. *Opt. Mater.* **2022**, *123*, 11906. [CrossRef]
4. Li, Z.; Cheng, Y.; Luo, H.; Chen, F.; Li, X. Dual-band tunable terahertz perfect bsorber based on all-dielectric InSb resonator structure for sensing application. *J. Alloys Compd.* **2022**, *925*, 166617. [CrossRef]
5. Feng, X.D.; Xie, X.; Pu, M.B. Hierarchical metamaterials for laser-infrared-microwave compatible camouflage. *Opt. Express* **2020**, *28*, 9445–9453. [CrossRef] [PubMed]
6. Garoil, D.; Calandrini, E.; Bozzola, A.; Toma, A.; Cattarin, S.; Ortolani, M.; Angelis, F.D. Fractal-like plasmonic metamaterial with a tailorable plasma frequency in the near-infrared. *ACS Photonics* **2018**, *5*, 3408–3414. [CrossRef]
7. Guo, L.Y.; Ma, X.H.; Zou, Y.G.; Zhang, R.; Wang, J.A.; Zhang, D. Wide-angle infrared metamaterial absorber with near-unity absorbance. *Opt. Laser Technol.* **2018**, *98*, 247–251. [CrossRef]
8. Pendry, J.B. Extremely low frequency plasmons in metallic mesostructures. *Phys. Rev. Lett.* **1996**, *76*, 4773–4776. [CrossRef]
9. Pendry, J.B.; Holden, A.J.; Robbins, D.J.; Steward, W.J. Magnetism from conductors and enhanced nonlinear phenomena. *IEEE Trans. Microw. Theory Tech.* **1999**, *47*, 2075–2084. [CrossRef]
10. Cheng, Q.; Cui, T.J.; Jiang, W.X.; Cai, B.G. An omnidirectional electromagnetic absorber made of metamaterials. *New J. Phys.* **2010**, *12*, 063006. [CrossRef]
11. Nie, G.Y.; Shi, Q.C.; Zhu, Z.; Shi, J.H. Selective coherent perfect absorption in metamaterials. *Appl. Phys. Lett.* **2014**, *105*, 201909. [CrossRef]
12. Üstün, K.; Gönül, T.S. Ultra-broadband long-wavelength infrared metamaterial absorber based on a double-layer metasurface structure. *J. Opt. Soc. Am. B* **2017**, *34*, 456–462. [CrossRef]
13. Zhong, M.; Jiang, X.T.; Zhu, X.L.; Zhang, J.; Zhong, J.L.; Chen, J.A.; Wu, S.X.; Zhang, J.H.; Liang, L.M.; Zeng, L.D.; et al. Enhancement of a tunable single-band metamaterial absorber based on bright–bright modes coupling effect in terahertz range. *Phys. Scr.* **2020**, *95*, 035508. [CrossRef]
14. Jain, P.; Singh, A.K.; Pandey, J.K.; Bansal, S.; Sardana, N. An Ultrathin compact polarization-sensitive triple-band microwave metamaterial absorber. *J. Electron. Mater.* **2021**, *50*, 1506–1513. [CrossRef]
15. Zhao, L. *Visible/Infrared Spectrum Matching Design and Control by Multiband Metamaterial Absorber*; School of Energy Science and Engineering: Harbin, China, 2021; pp. 96–118.
16. Wang, Z. *Research on 1550 nm High Power Pulsed Semiconductor Lasers*; University of Electronic Science and Technology of China: Chengdu, China, 2018; pp. 1–5.
17. Jiang, X. Polarization-Independent Wavelength Tunable Vertical Cavity Surface Emitting Laser Based on Two-dimensional Grating. *Chin. Opt. Lett.* **2019**, *39*, 320–324.
18. Paul, C.; Patrick, B.; Michael, V.; Emilie, S.; Nathalie, B.; Christophe, D.; Fabrice, P.; Riad, H. Experimental demonstration of the optical Helmholtz resonance. *Appl. Phys. Lett.* **2018**, *112*, 171110.
19. Li, P. *Study on the Radiation Absorption Characteristics of Solar Cell Surface Grating*; Huazhong University of Science and Technology: Wuhan, China, 2014; pp. 36–60.
20. Yang, X. *Study on 1.55 μm and 2 μm Tunable Fiber Lasers and Their Applications*; Zhejiang University: Hangzhou, China, 2020; pp. 31–40.
21. Liu, B.; Shi, J.M.; Zhang, J.K.; Li, Z.G.; Chen, Z.S.; Deng, X.S. Analysis of infrared stealth performance of photonic crystals with high heat dissipation. *Opt. Mater.* **2021**, *111*, 110689. [CrossRef]
22. Han, Y.X.; He, X.; Jie, J.L.; Yang, J.B.; Zhang, S. A mid-infrared narrowband absorber based on a subwavelength fine-structured silicon-gold metagrating. *Appl. Sci.* **2019**, *9*, 5022.

23. Sun, G.B.; Zhang, J.; Jiang, S.L.; Yang, L. Near-infrared absorption enhanced Ag nanopit-silicon gate composite structure simulation. *Adv. Lasers. Optoelectron.* **2022**, *59*, 0524001.

24. Pu, M.B.; Wang, C.T.; Wang, Y.Q.; Luo, X.G. Subwavelength Electromagnetics at Diffraction-Limited Scales. *Acta. Phys. Sin.* **2017**, *66*, 144101.

25. Lin, Y.F.; Hu, X.Q.; Hu, L. Realizing high-performance metamaterial absorber based on the localized surface plasmon resonance in the terahertz regime. *Mater. Res. Express.* **2018**, *5*, 045801.

26. Cui, Y.X.; He, Y.R.; Jin, Y.; Ding, F.; Yang, L.; Ye, Y.Q.; Zhong, S.M.; Lin, Y.Y.; He, S.L. Plasmonic and metamaterial structures as electromagnetic absorbers. *Laser. Photonics. Rev.* **2014**, *8*, 495–520. [CrossRef]

27. Palik, E.D. *Handbook of Optical Constants of Solids*; Academic Press: San Diego, CA, USA, 1985.

28. Landy, N.I.; Bingham, C.M.; Tyler, T.; Jokerst, N.; Smith, D.R.; Padilla, W.J. Design, theory, and measurement of a polarization insensitive absorber for terahertz imaging. *Phys. Rev. B* **2008**, *79*, 125104. [CrossRef]

29. Xie, Y.N.; Liu, X.Y.; Cai, Y.J.; Zhu, J.F. Polarization-insensitive dielectric metamaterial absorber for near-unity UV-light trapping in monolayer graphene. *Opt. Commun.* **2022**, *503*, 127459. [CrossRef]